Available online at www.sciencedirect.com
SCIENCE DIRECT®
Thin Solid Films 434 (2003) 171–177
thin solid films
www.elsevier.com/locate/tsf

Comparison of visible fluorescence properties between sol–gel derived Er^{3+}–Yb^{3+} and Er^{3+}–Y^{3+} co-doped TiO_2 films

San-Yuan Chen[a,*], Chu-Chi Ting[a], Wen-Feng Hsieh[b]

[a]*Department of Materials Science and Engineering, National Chiao-Tung University, 1001 Ta-hsueh Road, Hsinchu 300, Taiwan, ROC*
[b]*Institute of Electro-optical Engineering, National Chiao-Tung University, Hsinchu 300, Taiwan, ROC*

Received 24 September 2002; received in revised form 18 February 2003; accepted 18 February 2003

Abstract

Both Er^{3+}–Yb^{3+} and Er^{3+}–Y^{3+} co-doped TiO_2 films were prepared on fused silica by sol–gel processes. The effect of doping concentration upon the up-conversion fluorescence of Yb^{3+}–Er^{3+} and Er^{3+}–Y^{3+} co-doped TiO_2 systems will be focused in this investigation. Although the influence of Yb^{3+} and Y^{3+} ions on the structural of Er^{3+}–TiO_2 host material is almost the same, different up-conversion emissions are observed. Both Er^{3+}-doped and Er^{3+}–Y^{3+} co-doped TiO_2 films exhibit the up-conversion emission with green and red light. However, much stronger intensity of red light relative to green light is observed for the Er^{3+}–Yb^{3+} co-doped TiO_2 system. For Er^{3+} (5 mol%)–Y^{3+} co-doped TiO_2 samples, the relative intensity ratio (I_R/I_G) rapidly decreases with the increase of Y^{3+} concentration above 10 mol%. On the contrary, the relative intensity ratio (I_R/I_G) increases with increasing Yb^{3+} concentration for Er^{3+} (5 mol%)–Yb^{3+} co-doped TiO_2 samples. The up-conversion emission in the Er^{3+}–Y^{3+} co-doped TiO_2 system belongs to a two-photon absorption up-conversion process. However, the overall up-conversion efficiency in the Er^{3+}–Yb^{3+} co-doped TiO_2 system could be contributed from the complicated mechanisms.

Keywords: Titanium oxide; Up-conversion; Sol–gel; Raman scattering

1. Introduction

Some rare-earth ions, when incorporated as impurities in sufficient concentration into suitable host materials, can up-convert infrared radiation into various shorter wavelengths [1,2]. This process plays an important role in enhancing optical detection and display devices. Over the past two decades, a number of papers have accumulated in search of new materials with high up-conversion efficiency [3–6]. For instance, numerous systems with Er^{3+} ions doped have been thoroughly studied in glasses [3], fiber amplifiers [4], sol–gel glass [5] and crystals [6]. However, when developing the rare-earth-doped optical devices, the optical properties of the host materials have to be considered since the efficiency of up-conversion strongly depends on the crystal-field strength and lattice vibration of host matrices.

Amorim et al. reported that low-phonon energy and high refractive index of sulfide-based chalcogenide glasses can reduce the nonradiative decay rates of rare-earth energy levels, and enhance the radiative emission rates [7]. Similarly, TiO_2 thin film was reported to have higher refraction index ($n=2.52$ for anatase and $n=2.76$ for rutile) as well as lower phonon energy (<700 cm^{-1}) [8] than silica glass film. Recently, it has been demonstrated that Er^{3+}-doped TiO_2-based films have potential applications in the micro-integrated photonic devices [9,10]. Furthermore, in our previous report, we have demonstrated that by codoping yttrium into the Er^{3+}-doped TiO_2-based films, the $\sim$1.54 μm PL properties can be enhanced by a factor of 10 times for intensity and 1.5 times for full width at half maximum in comparison with the Er^{3+}–Al^{3+} co-doped SiO_2 system [11]. The enhanced PL emission of the Er^{3+}–Y^{3+} co-doped TiO_2 films is attributed to the sufficient dispersion and distorted local structure of Er^{3+} ions in TiO_2 host matrix. In contrast to Y^{3+} ions, Yb^{3+} ions act as sensitizers in heavily Er-doped silica optical fibers

*Corresponding author. Tel.: +886-3-5731818; fax: +886-3-5724727.
E-mail address: sychen@cc.nctu.edu.tw (S.-Y. Chen).

0040-6090/03/$ - see front matter © 2003 Elsevier Science B.V. All rights reserved.
doi:10.1016/S0040-6090(03)00456-5

because Yb^{3+} ions can more efficiently absorb the 980 nm light and transfer the energy to Er^{3+} ions [12]. This mechanism makes the population of $^4I_{11/2}$ Er^{3+} level increase and leads to the enhancement of ~1.54 μm PL efficiency.

Recently, it has been proposed by some investigators that multi-ion doped systems can be utilized to enhance up-conversion efficiency [13,14]. For example, relatively high up-conversion efficiency through energy transfer has been reported for BaF_2–ThF_2 glass systems with Yb^{3+}/Er^{3+} and Yb^{3+}/Tm^{3+} co-doped [14]. On the other hand, it has been known that these $Yb^{3+}/Y^{3+}/Er^{3+}$ ions have similar ionic radii ($Yb^{3+}=0.0862$ nm, $Y^{3+}=0.0892$ nm and $Er^{3+}=0.0881$ nm) and $Yb_2O_3/Y_2O_3/Er_2O_3$ have nearly the same crystal structural. However, Yb^{3+} and Y^{3+} belong to different chemical groups. Yb is characteristic of intra-4*f* transition and the outer closed $5s^25p^6$ shells screen the unfilled inner $4f^{11}$ shell but Y does not have intra-4*f* transition orbital [15,16]. Furthermore, up to now, little or no attention has been directed to the up-conversion characteristics of Er^{3+}-doped TiO_2 ceramics [17].

Therefore, in this work, the Yb^{3+}or Y^{3+} ions have been tried to co-doped into co-doped TiO_2 systems. The effect of doping concentration upon the up-conversion fluorescence will be studied for both co-doped TiO_2 systems. Further comparison of up-conversion fluorescence was investigated to clarify the role of Yb^{3+} and Y^{3+} codopants in Er^{3+}-doped TiO_2 based on structural similarity and different characteristics between Yb^{3+} and Y^{3+}.

2. Experimental procedure

2.1. Sample preparation

Acetic acid (HAc, Merck) and 2-methoxyethanol (MOE, Merck) with molar ratio of Ti/HAc/MOE=1/10/15 were first added to titanium isoproxide (Alfa), followed by stirring for 30 min. Subsequently, the ytterbium acetate (or yttrium acetate) (Alfa) and erbium acetate (Alfa) powders were dissolved into the titanium solution and stirred for 10 h to process homogeneous hydrolysis/polymerization reaction. The molar ratios of Er^{3+}/Ti^{4+} and Yb^{3+} (or Y^{3+})/Ti^{4+} were varied from 0.5 to 10 mol% and 10 to 50 mol%, respectively.

For the thin film fabrication, the Er^{3+}–Yb^{3+} co-doped TiO_2 precursor solution was spin-coated on fused silica substrates. The as-deposited sol–gel films were first pyrolyzed under dry oxygen atmospheres at 400 °C for 30 min at a heating rate of 3 °C/min and then annealed at temperatures ranging from 700 to 1000 °C for 1 h in dry oxygen atmosphere. Multiple spin-coating processes were employed to deposit ~0.5 μm thick films. For comparison purpose, the Er^{3+}–Y^{3+} co-doped TiO_2 films following the same procedure were also fabricated.

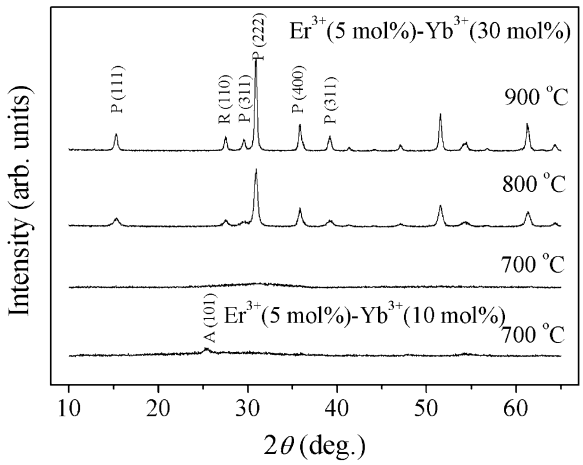

Fig. 1. XRD patterns of Er^{3+}–Yb^{3+}(10 or 30 mol%) co-doped TiO_2 annealed from 700 to 900 °C for 1 h.

2.2. Characterization measurements

The phase structure of samples was analyzed by X-ray diffractometer using Cu Kα radiation. A 980 nm diode laser with power of 50 mW was used as the pump source inclined 45° to irradiate the samples. The fluorescence spectra were recorded normally from the samples at room temperature using a spectrophotometer (ARC) equipped with a liquid N_2-cooled Ge detector for the detection of infrared fluorescence, and a multi-alkali photomultiplier tube for the detection of visible fluorescence. The Raman spectrum was recorded on a Jobin-Yvon T6400 instrument with an Ar^+ laser source of 514 nm wavelength and an incident power of 2 mW mm^{-2}.

3. Results and discussion

3.1. Structural evolution

The X-ray diffraction (XRD) patterns in Fig. 1 show that the effect of annealing temperatures on structural evolution of Er^{3+}(5 mol%)–Yb^{3+}(10 or 30 mol%) co-doped TiO_2. At 700 °C, the anatase TiO_2 phase can be detected for the sample with 10 mol% Yb^{3+} codoping but when the concentration of Yb^{3+} ions increases more than 10 mol%, the host matrix becomes amorphous. As the samples are further annealed at 800 °C, the well-crystallized pyrochlore crystallite $Er_xYb_{2-x}Ti_2O_7$ has been generated within the TiO_2 host matrix. Similar results are also observed in the Er^{3+}–Y^{3+}co-doped TiO_2 system because the ionic radius of both Yb^{3+} and Y^{3+} ions is very similar to that of Er^{3+} ion. It is interesting to note that $Er_2Ti_2O_7$, $Yb_2Ti_2O_7$ and

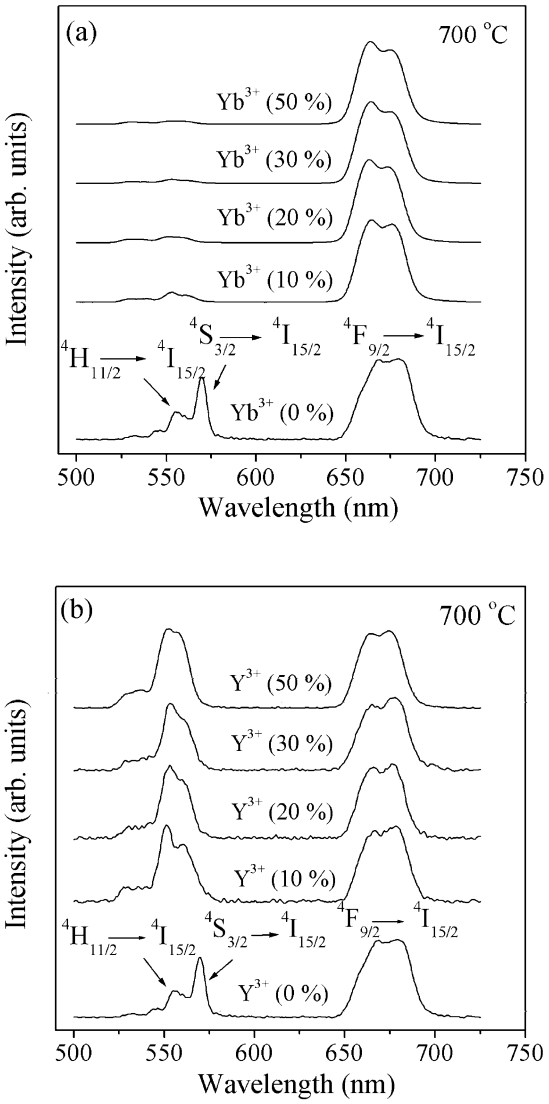

Fig. 2. Up-conversion spectra of (a) Er^{3+} (5 mol%)–Yb^{3+} (0–50 mol%) (b) Er^{3+} (5 mol%)–Y^{3+} (0–50 mol%) co-doped TiO_2 samples annealed at 700 °C for 1 h. All of the spectra were normalized on the same basis on intensity for comparison among spectral features.

$Y_2Ti_2O_7$ pyrochlore phases have the same crystal structure and similar lattice constant. Therefore, pyrochlore phases in Er^{3+}–Yb^{3+} or Er^{3+}–Y^{3+} co-doped TiO_2 samples can be regarded as $Er_2Yb_{2-x}Ti_2O_7$ or $Er_2Y_{2-x}Ti_2O_7$, where Er^{3+}, Yb^{3+} and Y^{3+} ions are structurally indistinguishable. In the pyrochlore phase such as $Yb_2Ti_2O_7$, Ti^{4+} ions are six coordinated and are located within trigonal antiprisms with all the six anions at equal distance from the central Ti^{4+} cations. However, Er^{3+} (Y^{3+} or Yb^{3+}) ions are eight coordinated and located within scalenohedra (distorted cubes) that contain six equal-space anions at a slightly shorter distance from the central Er^{3+} (Y^{3+} or Yb^{3+}) cations [18]. The aforementioned local structural evolution of Er^{3+} ions can considerably influence the photoluminescence properties of Er^{3+}–Yb^{3+} (or Er^{3+}–Y^{3+}) co-doped TiO_2 systems.

3.2. Up-conversion properties

Fig. 2 shows the up-conversion luminescence in the 500–700 nm range for Er^{3+} (5 mol%)–Yb^{3+} (or Y^{3+}) co-doped TiO_2 samples annealed at 700 °C h^{-1}. According to the Er^{3+} ion energy level diagram, these visible fluorescence spectra exhibit the bands at approximately 569 and 554 nm which are identified as the $^4S_{3/2} \rightarrow {}^4I_{15/2}$ and $^4H_{11/2} \rightarrow {}^4I_{15/2}$ transitions, as well as the band at approximately 660 nm corresponding to the $^4F_{9/2} \rightarrow {}^4I_{15/2}$ transition.

Obviously, there exists remarked difference between Er^{3+}–Yb^{3+} and Er^{3+}–Y^{3+} co-doped TiO_2 systems. Both Er^{3+}-doped and Er^{3+}–Y^{3+} co-doped TiO_2 films exhibit the up-conversion emission with green and red light. However, much stronger intensity of red light relative to green light is observed in the Er^{3+}–Yb^{3+} co-doped TiO_2 system. Fig. 3 shows the relative intensity ratio of I_R/I_G (where I_R and I_G represent the intensities of red and green up-converted emission, respectively) as a function of Y^{3+} or Yb^{3+} concentration in Er^{3+} (5

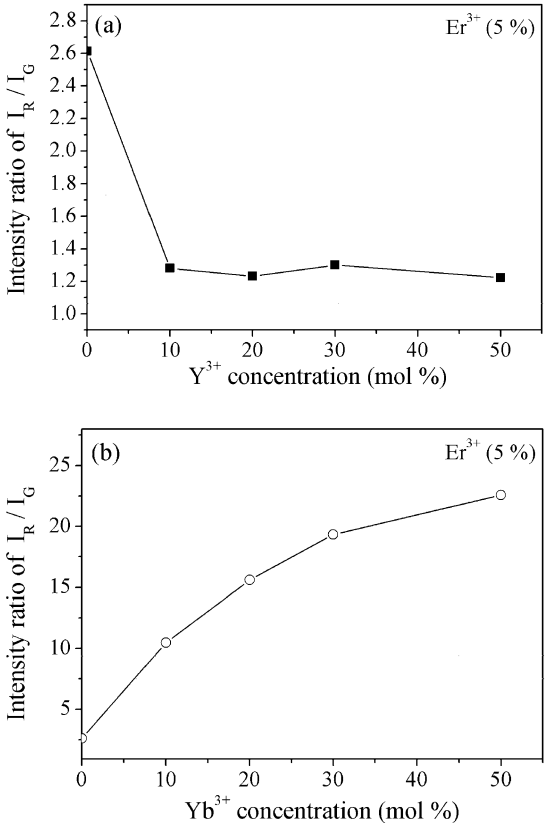

Fig. 3. Intensity ratio of I_R/I_G as a function of codopant concentration in (a) Er^{3+} (5 mol%)–Y^{3+} and (b) Er^{3+} (5 mol%)–Yb^{3+} co-doped TiO_2 systems (where I_R and I_G represents the intensity of red and green up-converted emission).

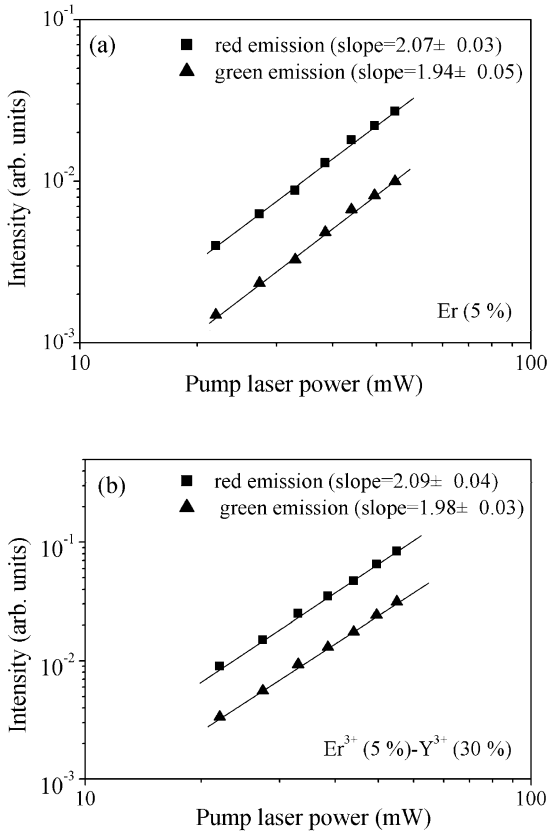

Fig. 4. Intensities of both green and red up-converted emissions vs. the pump power for the (a) Er^{3+} (5 mol%)-doped and (b) Er^{3+} (5 mol%)–Y^{3+} (30 mol%) co-doped TiO_2 systems annealed at 700 °C h^{-1}.

mol%)–Y^{3+} and Er^{3+} (5 mol%)–Yb^{3+} co-doped TiO_2 systems. By codoping Y^{3+} ions, the relative intensity ratio (I_R/I_G) decreases from ~2.6 to an approximately fixed value of ~1.3 for Er^{3+} (5 mol%)-doped TiO_2 samples with Y^{3+} concentration above 10 mol%. On the contrary, the relative intensity ratio (I_R/I_G) increases with increasing Yb^{3+} concentration for Er^{3+} (5 mol%)–Yb^{3+} co-doped TiO_2 samples. In addition, the influence of Y^{3+} or Yb^{3+} concentration on the line shape of visible fluorescence is not so pronounced, which was also observed in Er^{3+}–Al^{3+} co-doped SiO_2 system [5].

For the Er^{3+}-doped and Er^{3+}–Y^{3+} co-doped TiO_2 samples annealed at 700 °C for 1 h, the intensity of both green and red up-conversion emissions vs. the pump power at 980 nm has been plotted in Fig. 4. The slope in Fig. 4 is approximately equal to 2 on a log–log scale. This result confirms that green and red emissions belong to a two-photon absorption up-conversion process [19–21]. However, a slope of 1.5 for the Er^{3+}–Yb^{3+} co-doped TiO_2 samples shown in Fig. 5 indicates that the mechanism is not a biphotonic case. The dependence of the overall green and red up-conversion intensity (I_R+I_G) on codopant concentration

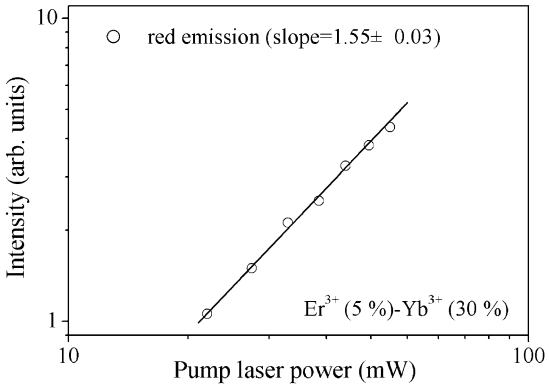

Fig. 5. Intensities of red up-converted emissions vs. the pump power for the Er^{3+} (5 mol%)–Yb^{3+} (30 mol%) co-doped TiO_2 systems annealed at 700 °C/1 h.

is summarized in Fig. 6 for both Er^{3+} (5 mol%)–Yb^{3+} and Er^{3+} (5 mol%)–Y^{3+} co-doped TiO_2 samples annealed at 700 °C/1 h. The Er^{3+} (5 mol%)–Yb^{3+} co-doped TiO_2 system has the much higher up-conversion efficiency than Er^{3+} (5 mol%)–Y^{3+} co-doped TiO_2 system.

The influence of annealing temperatures (from 700 to 1000 °C) on an up-conversion emission is shown in Fig. 7 for Er^{3+} (5 mol%)-doped, Er^{3+} (5 mol%)–Y^{3+} (30 mol%) co-doped and Er^{3+} (5 mol%)–Yb^{3+} (30 mol%) co-doped TiO_2 systems. As the samples were annealed above 800 °C, these spectra show a common feature. In other words, a broad red emission splits into two peaks and the relative intensity ratio (I_R/I_G) slightly increases with the increase of annealing temperatures or the formation of pyrochlore phase.

The multiphonon relaxation processes are directly related to the phonon energy of host materials and

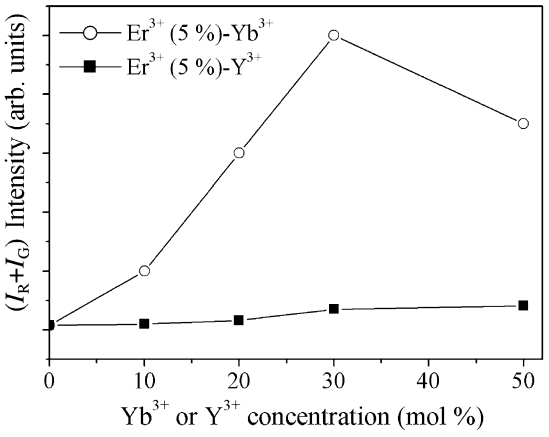

Fig. 6. Dependence of the overall green and red up-conversion intensity (I_R+I_G) on the codopant concentration for Er^{3+} (5 mol%)–Yb^{3+} and Er^{3+} (5 mol%)–Y^{3+} co-doped TiO_2 systems annealed at 700 °C/1 h (where I_R and I_G represent the intensity of red and green up-converted emission).

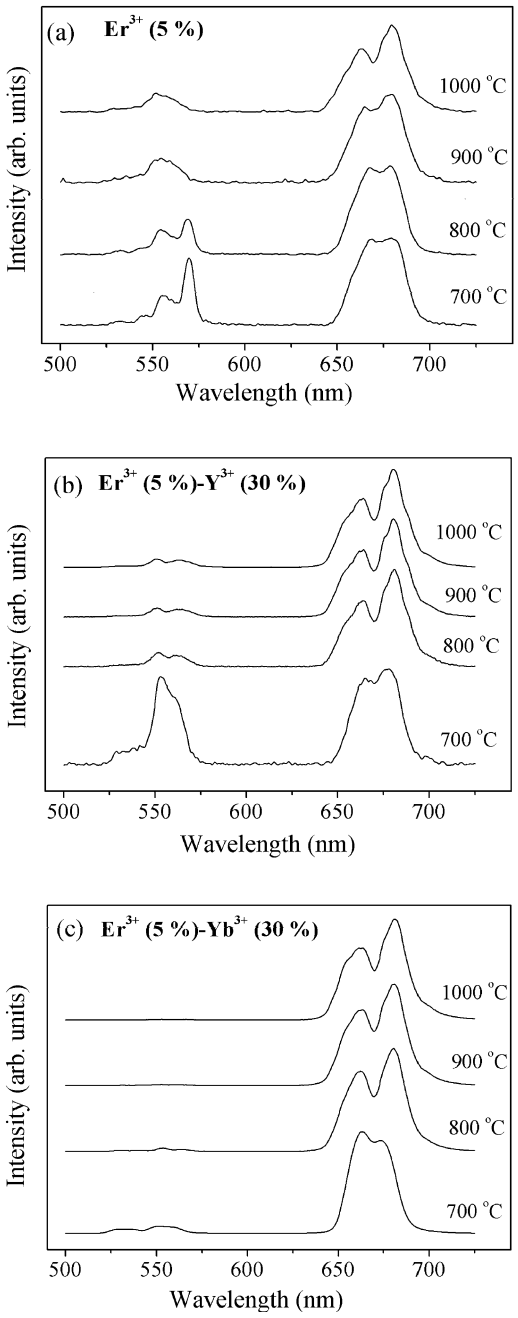

Fig. 7. Up-conversion spectra of (a) Er^{3+} (5 mol%)-doped; (b) Er^{3+} (5 mol%)–Y^{3+} (30 mol%) co-doped and; (c) Er^{3+} (5 mol%)–Yb^{3+} (30 mol%) co-doped TiO_2 samples annealed from 700 to 1000 °C for 1 h. All of the spectra were normalized on the same basis on intensity for comparison among spectral features.

characteristics of codopant (e.g. concentration, crystal field and sensitizing) [22]. Low-energy phonon materials prevent de-excitation of the excited-state levels through non-radiative phonon-assisted relaxation that results in a strongly enhanced luminescent quantum yield for near infrared radiation into visible light through frequency up-conversion [7,13]. Fig. 8 illustrates that

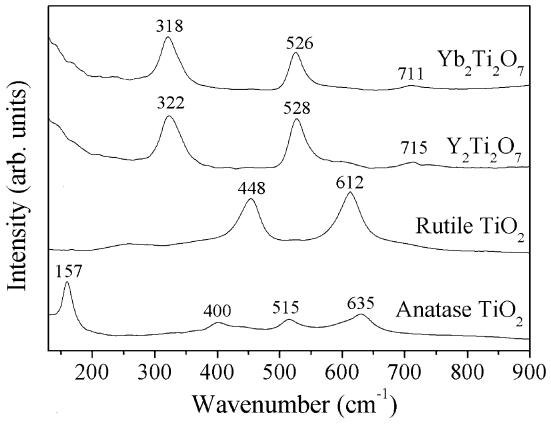

Fig. 8. Raman spectra of anatase, rutile, $Y_2Ti_2O_7$ and $Yb_2Ti_2O_7$.

anatase TiO_2 shows a strong Raman band at 157 cm^{-1} and weak bands at 400, 515 and 635 cm^{-1}. The bands of rutile TiO_2 are at 612, 448 and 240 cm^{-1} [24]. Generally, the bands approximately 157 and 612 cm^{-1} are used to identify anatase and rutile phases, respectively. Both $Yb_2Ti_2O_7$ and $Y_2Ti_2O_7$ pyrochlore phases

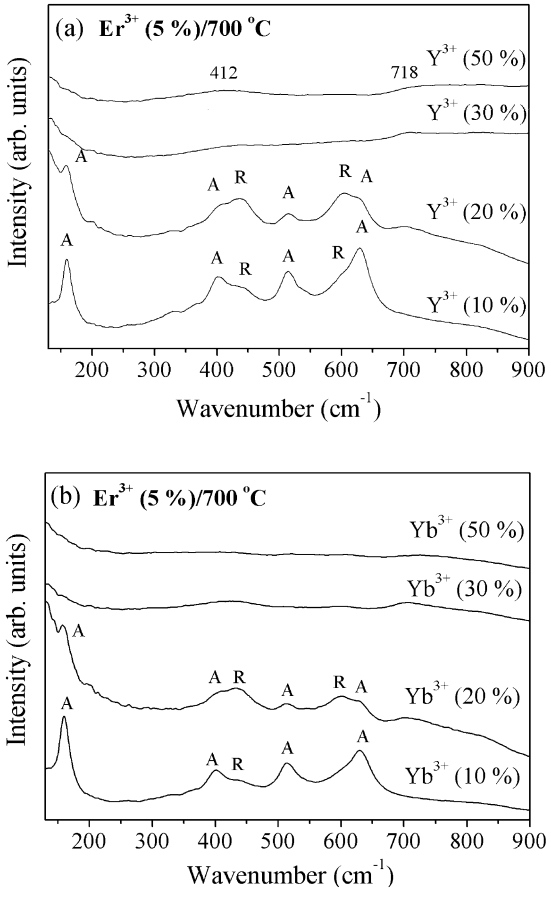

Fig. 9. Raman spectra of (a) Er^{3+} (5 mol%)–Y (10–50 mol%) and (b) Er^{3+} (5 mol%)–Yb (10–50 mol%) co-doped TiO_2 annealed at 700 °C for 1 h.

exhibit very similar Raman spectra and the maximum phonon energies are located approximately 710–720 cm^{-1}. The Raman spectra (Fig. 9a) in the Er^{3+} (5 mol%)–Y^{3+} (10–50 mol%) co-doped TiO_2 samples annealed at 700 °C/1 h illustrate that 30–50 mol% Y codopant can result in the amorphous host matrix with two weak and broad bands approximately 412 and 718 cm^{-1}. However, the host matrix with mixed anatase and rutile phases is observed for 10–20 mol% Y codopant. Similar phenomenon as shown in Fig. 9b is also detected for Er^{3+} (5 mol%)–Yb^{3+} (10–50 mol%) co-doped TiO_2 system. As the samples were annealed above 800 °C, the Raman spectra (no shown here) reveal that both Er^{3+} (5 mol%)–Yb^{3+} (30 mol%) and Er^{3+} (5 mol%)–Y^{3+} (30 mol%) co-doped TiO_2 systems have very similar phonon energy. Therefore, the influence of multiphonon relaxation processes on the up-conversion efficiency for these two systems is almost the same, which indicates that the up-conversion efficiency is mainly determined by the characteristics of codopant.

In general, there are two kinds of up-conversion mechanisms [4,23,24]: excited-state absorption (ESA) and energy-transfer up-conversion (ETU). In the Er^{3+}(5 mol%)–Y^{3+} (10–50 mol%) co-doped TiO_2 system, the intensity of visible fluorescence presents a quadratic dependence on infrared pump intensity, which suggests that the possible up-conversion excitation mechanism is the two-photon absorption followed by phonon-assisted energy transfer. The I_R/I_G intensity ratio has an approximately fixed value of ~1.3, which means that the probability of nonradiative phonon-assisted decay from $^4F_{7/2}$ to green emitting levels ($^4H_{11/2}$ and $^4S_{3/2}$) and to red emitting level ($^4F_{9/2}$) is similar. On the other hand, a very strong intensity of the red emission with a power dependence of 1.5 is observed in the Er^{3+} (5 mol%)–Yb^{3+} (10–50 mol%) co-doped TiO_2 system, which also occurs in Er^{3+}–Yb^{3+} co-doped SiO_2 system. The lack of simple power dependence is not surprising since several excitation mechanisms appear to be involved. Except for the ESA, Er^{3+}–Er^{3+} ETU and Yb^{3+}–Er^{3+} double energy transfer mechanisms can produce the red emission. Furthermore, the other two main up-conversion paths as shown in Fig. 10 also contribute to the red emission [25,26]. Because the Er^{3+} excited state level $^4I_{11/2}$ might be saturated by the energy transfer of Yb^{3+} ($^4F_{5/2}$) electrons in this $^4I_{11/2}$ level and relax to $^4I_{13/2}$ level through a multi-phonon relaxation and then the $^4F_{9/2}$ level is populated via ESA of pump photons. The other mechanism is that the Er^{3+} excited state level $^4F_{7/2}$ is deexcited to the $^4F_{9/2}$ accompanied with raising the other state level from $^4I_{11/2}$ to $^4F_{9/2}$ through an energy transfer cross-relaxation. The above two extra mechanisms can make the $^4F_{9/2}$ level more populated. Therefore, the final obtained up-conversion efficiency can be summarized from the overall contributions of the five mechanisms which result in a very strong red emission in Er^{3+}–Yb^{3+} co-doped TiO_2 system compared to Er^{3+}–Y^{3+} co-doped TiO_2 system.

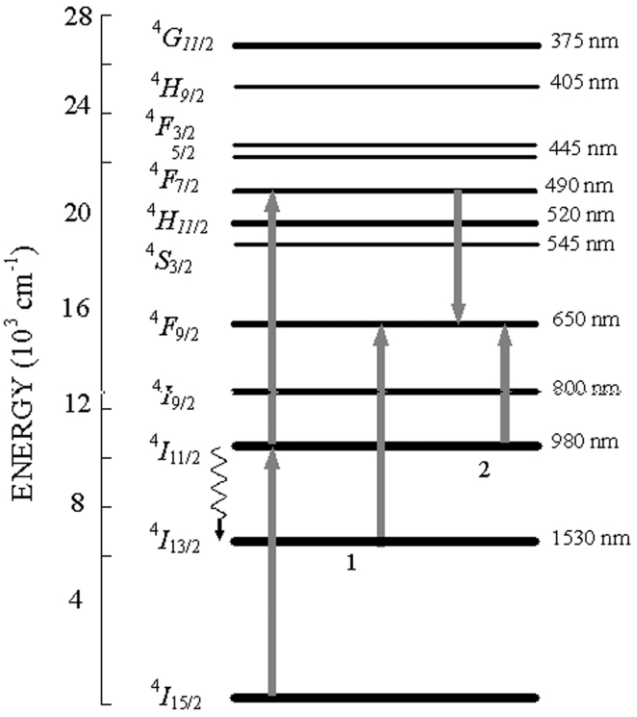

Fig. 10. Schematic up-conversion mechanism of the Er^{3+} ESA under 980 nm pumping.

4. Conclusions

Both Er^{3+}–Yb^{3+} and Er^{3+}–Y^{3+} co-doped TiO_2 films were prepared on fused silica by sol–gel processes. The influence of Yb^{3+} and Y^{3+} ions on the structural and phase development of Er^{3+}–TiO_2 host material is almost the same. Both Er^{3+}-doped and Er^{3+}–Y^{3+} co-doped TiO_2 samples exhibit the up-conversion emission with green and red light. For Er^{3+} (5 mol%)–Y^{3+} co-doped TiO_2 system, the relative intensity ratio (I_R/I_G) rapidly drops with the increase of Y^{3+} concentration above 10 mol%. On the contrary, the relative intensity ratio (I_R/I_G) increases with increasing Yb^{3+} concentration for Er^{3+} (5 mol%)–Yb^{3+} co-doped TiO_2 system. In addition, the up-conversion emission in the Er^{3+}–Y^{3+} co-doped TiO_2 system belongs to a two-photon absorption up-conversion process that is different from that of Er^{3+}–Yb^{3+} co-doped TiO_2 system.

Acknowledgments

This work was financially supported by the National Science Council of the Republic of China, Taiwan under Contract No. NSC90-2216-E-009-041.

References

[1] T.J. Whitley, C.A. Millar, R. Wyatt, M.C. Brierley, D. Szebesta, Electron. Lett. 27 (1991) 1785.
[2] F. Auzel, P. Pecile, D. Morin, J. Electrochem. Soc. 122 (1975) 101.
[3] E. Snoeks, G.N. van den Hoven, A. Polman, B. Hendriksen, M.B.J. Diemeer, F. Priolo, J. Opt. Soc. Am. B 12 (1997) 1468.
[4] P. Blixt, J. Nilsson, T. Carlnas, B. Jaskorzynska, IEEE Photon. Technol. Lett. 2 (1991) 3.
[5] B.T. Stone, K.L. Bray, J. Non-Cryst. Solids 197 (1996) 136.
[6] H. Nii, K. Ozaki, M. Herren, M. Morita, J. Lumin. 76–77 (1998) 116.
[7] H.T. Amorim, M.T. de Araujo, E.A. Gouveia, A.S. Gouveia-Neto, J.A.M. Neto, A.S.B. Sombra, J. Lumin. 78 (1998) 271.
[8] C. Urlacher, J. Mugnier, J. Raman Spectrosc. 27 (1996) 785.
[9] A. Bahtat, M. Bouazaoui, M. Bahtat, J. Mugnier, Opt. Commun. 111 (1994) 55.
[10] A. Bahtat, M. Bouderbala, M. Bahtat, M. Bouazaoui, J. Mugnier, M. Druetta, Thin Solid Films 323 (1998) 59.
[11] C.C. Ting, S.Y. Chen, W.-F. Hsieh, H.-Y. Lee, J. Appl. Phys. 90 (2001) 5564.
[12] A.F. Obaton, C. Labbé, P.L. Boulanger, B. Elouadi, G. Boulon, Spectro. Acta A 55 (1999) 263.
[13] C.B. Layne, W.H. Lowdermilk, M.J. Weber, Phys. Rev. B 16 (1997) 10.
[14] Y. Mita, T. Ide, M. Togashi, H. Yamamoto, J. Appl. Phys. 85 (1999) 4160.
[15] H. Ennen, J. Schneider, G. Pomrenke, A. Axmann, Appl. Phys. Lett. 43 (1983) 943.
[16] H. Ennen, G. Pomrenke, A. Axmann, K. Eisele, W. Haydl, J. Schneider, Appl. Phys. Lett. 46 (1985) 381.
[17] A. Bahtat, M. Bouazaoui, M. Bahtat, C. Garapon, B. Jcaquier, J. Mugnier, J. Non-Cryst. Solids 202 (1996) 16.
[18] M.A. Subramanian, G. Aravamudan, G.V. Subba Rao, Prog. Solid St. Chem. 15 (1983) 55.
[19] E. Maurice, G. Monnom, B. Dussardier, D.B. Ostrowsky, J. Opt. Soc. Am. B 13 (1996) 693.
[20] J.L. Jackel, A.Y. Yan, E.M. Vagel, A.V. Lehmen, J.J. Johnson, E. Snitzer, Appl. Opt. 31 (1992) 3390.
[21] N. Jaba, A. Kanoun, H. Mejri, S. Alaya, H. Maaref, J. Phys.: Condens. Matter. 12 (2000) 4523.
[22] S. Tanabe, S. Yoshii, K. Hirao, N. Soga, Phys. Rev. B 45 (1992) 4620.
[23] N. Floquet, O. Bertrand, J.J. Heizmann, Oxidation Met. 37 (1992) 253.
[24] M.P. Hehlen, G. Frei, H.U. Güdel, Phys. Rev. B 50 (1994) 16264.
[25] F. Goutaland, Y. Querdane, A. Boukenter, G. Monnom, J. Alloys Compd. 275–277 (1998) 276.
[26] N. Jaba, A. Kanoun, H. Mejri, S. Alaya, H. Maaref, J. Phys.: Condens. Matter. 12 (2000) 4523.